A Friction Model for Laminator Nips

Stefan Oros

LUND
UNIVERSITY

Department of Automatic Control

MSc Thesis
ISRN LUTFD2/TFRT--5968--SE
ISSN 0280-5316

Department of Automatic Control
Lund University
Box 118
SE-221 00 LUND
Sweden

Printed in Sweden by Tryckeriet i E-huset
Lund 2015

Abstract

The main objective for the thesis project is to find a suitable mathematical model of the velocity dependent friction force that arises between the nip roller and the carton material in the laminator at slip, in order to enable realistic simulations of the nip in the laminator. Theoretically, the *LuGre* model is found to contain the necessary physical properties for the actual situation. Experiments are conducted measuring friction between a rubber sample and carton samples in order to find an expansion and validation of the model. The model is found to produce a satisfactory low-magnitude residual in relation to the experiments for the range that varies with velocity. During the low velocities high-amplitude friction induced oscillations appear making the measurements highly inaccurate. It is known, however, that the slip will never reach these low velocities so this source of error is disregarded. Also, the measurement instrument is found not to be entirely ideal for this project. An instrument that can continuously change the velocity would be better. This model is good for most of the nip cases. However, further investigations are needed for the boundary effects that arise due to the cylindrical shape of the rollers and also a way to identify the dynamical parameters and thus expand from a steady-state model to a dynamical model.
Keywords: friction, LuGre, modelling, Stribeck, sliding, carton

In loving memory of my grandmother Elena, who always gave me immense joy and motivation during my studies.

Acknowledgements

First of all I would like to give my warmest gratitude to my two supervisors, Dr. Rolf Johansson at Automatic Control and Martin Adell at Tetra Pak, for their unlimited aid and excellence in the field during this project. Further, I would like to thank Mattias Månsson, Tetra Pak, for the invaluable help with modelling and simulations. I would also like to thank Karin Strömberg, my mentor during the Technical Talent program that lead to this thesis.

Finally, I am infinitely grateful to my family and friends for their endless support and care during my time at the university.

Contents

List of Figures

1

Introduction

1.1 Background and motivation

Tetra Pak is a world-leading manufacturer of packaging materials for consumables. A set of physical properties and process parameters when laminating paper board influence the properties of the final package. This thesis will focus on a part of the laminator called the Nip. The Nip is where a pressure rubber roller and a metal chill roller meet and thus friction will be a physical phenomenon affecting the process.

1.2 Objectives

The general goal is to find a suitable mathematical model describing the friction phenomenon appearing in the nip. Since it is not only the rubber roller versus the chill roller but an actual material being pressed in between, several questions as well as difficulties arise. How does the choice of material affect the model? What parameters influence the model, that is, what parameters will be dominant in the model? Can the model be generalised? The objectives of this thesis are:

- Find a mathematical model that takes velocity as input and gives a kinetic friction coefficient as output.

- Find a way to calibrate the model according to performed measurements in order to acquire adequate values for the kinetic coefficient of friction at different sliding velocities.

2

Theory

Sliding friction is one of the problems that experience a very long history of research in physics. It is also of great importance in research and engineering. In some industries the aim is to increase friction force (e.g. tires) and in other industries the aim is to decrease the friction (e.g. wear caused by friction). One of the oldest examples of using friction for practical use dates all the way back to around 200 000 BC when the neanderthals discovered how to generate fire by the use of friction between wood objects or flint stones. According to [Persson, 1998] the estimated monetary losses in the USA due to disregarding tribology (the science of interacting surfaces, in which friction research is vital) are 6% of its GNP - that is 420 billion USD.

This section covers what is necessary to know in order to comprehend the very complex phenomenon of friction and the modelling of friction.

2.1 Friction

The brief historical review of friction in this section is based on [Popov, 2010].
Coulomb friction, also named *dry friction*, between two bodies in contact is a complex physical phenomenon to study as it is affected by several factors. When the two bodies are in motion relative to each other there is a force resisting the motion - the friction force. The first known study of friction is the work of *Leonardo Da Vinci*, Codex-Madrid I, in 1495. In this work Da Vinci empirically derived some basic laws of friction:

1. The friction force is proportional to the normal force (applied load).
2. The friction force is independent of the surface area.

These laws were discovered again by Guillame Amontons in 1699, and thus the first law is also named *Amonton's law*. In 1750, Leonard Euler approached friction in a more theoretical manner where he proposed that friction was caused by interlocking irregularities between the body surfaces. In this work he distinguished static

friction from kinetic friction and also introduced the *coefficient of friction* μ [Popov, 2010]. In 1781 Charles Augustin Coulomb published a study on dry friction which still today is viewed as the core of tribology and friction. In this he did confirm Amonton's laws and also added a third law:

3. The friction force is independent of the sliding velocity.

The theory of tribology, friction and wear has then evolved during the following 230 years, much due to the works on contact mechanics by Hertz in the 19th century and Tabor & Boden in the mid 20th century. The later pioneered in proposing a more detailed physical theory of the cause of friction. They investigated the surface and explained that friction is caused by asperities being in contact with each other and thus when in motion they deform elastically and plastically [Bowden and Tabor, 1950]. The theory contains a true contact area which is a lot smaller than the apparent surface area. Thus, if applying a larger load to the body, the true contact area will increase and so the amount of asperities being in contact with each other - hence the friction force will increase. A more in-depth theoretical presentation follows below in the following section.

2.2 Tribotechnical system

Tribology is the name of the research field concerning surfaces interacting with each other included solids, liquids and gases. The main point of tribology, and the actual reason as of why it is so important for engineers, is to optimize friction and wear for the application worked with. Friction - which the objective of this study is to model - depends on several factors. However, it is important to understand that friction is not to be viewed as the property of a specific material but more the property of an entire system. This can be illustrated in a tribotechnical system (TTS). The system is modelled as a *black box system* as seen in Fig. 2.1.

The idea of doing this is to put the attributes that are directly involved in friction, such as the materials and geometries of the actual moving bodies, in the black box and thus isolating them from the rest of the system. The meaning of this is to achieve a function where the input variables are converted into usable output variables. Added to input variables are usually also disturbance variables that do influence the output variables as well as the loss variables. Loss variables can e.g. be mechanical energy converted to vibrations or heat.

Black Box Structure

Within the black box is the so called structure, which describes the elements involved and the interaction between them, see Fig. 2.2. There are four elements: Main body, counterbody, interfacial medium and ambient medium. The main and counter bodies are always present in the structure. However not all contain an interfacial or ambient medium (the latter if the system is placed in vacuum). There are

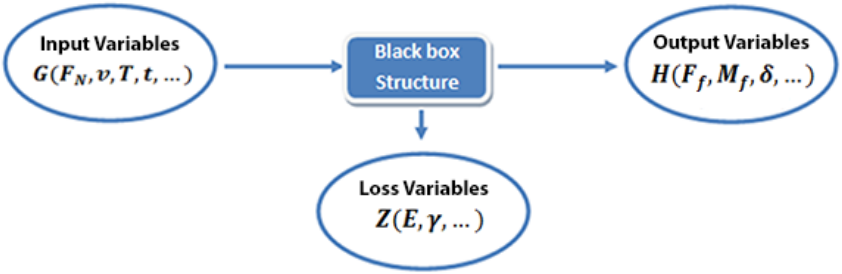

Figure 2.1 A TTS illustrated as a black box system. Also disturbance variables can be added for correction purposes.

.

two main ways to tell apart different systems – *closed* and *open systems*. If the base body is constantly stressed by new material zones of the counter body it is called an open system. The function in these systems mainly depends on the wear of the base body, since the counter body generates the load. If, on the contrary, the stressed zones of the base body and counter body are repeatedly in contact, then the system is closed. In these systems the function depends on the wear of both bodies.

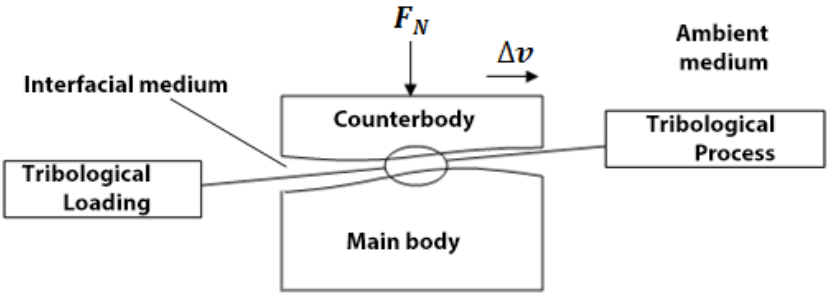

Figure 2.2 The black box of the TTS – the structure. The elements are directly involved in friction and wear.

2.3 The Contact Area

From a macroscopic point of view a surface might seem nominally flat, however, it is common knowledge that any surface is very uneven microscopically both due to asperities and waviness. Thus it is essential to look at the topography since the

asperity contacts and waviness are the key to friction and wear. The total contact area, A_C, usually called real contact area, is the sum of the all the areas of the asperities that are in contact with the opposing body, $A_C = \sum_{i=1}^{n} A_{C,i}$, see Fig. 2.3. The total is obviously highly dependent on the surface roughness distributions and separation of the two bodies. The real area of contact is significantly smaller than the nominal area of contact. This also means that the pressure over the asperity contacts are higher than the nominal pressure implying that even if the material is still behaving elastically on a macroscopic level plasticity might already have occurred on a microscopic level [Bowden and Tabor, 1964].

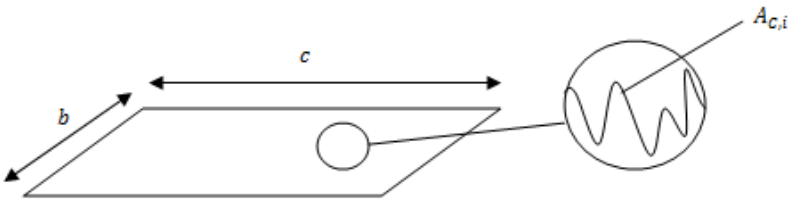

Figure 2.3 On a microscopic level any surface consists of asperities.

2.4 Load and interactions in the structure

Input and disturbance variables impact on the structure give rise to tribological load in a TTS - which mainly includes contact, kinematic and thermal processes. This has several impacts on the system. Normally, the tips of the asperities are approximated to be spherical in shape and perfectly smooth and that the counterpart is plane [Bowden and Tabor, 1950], see Fig. 2.4. If we suppose that the surfaces are pushed together by a load W, according to Hertz contact equations (see [Popov, 2010] for a review of the Hertz contact theory) they will deform elastically until the yield strain is reached. The region of contact, A_C, is bounded by a circle with a radius a, given by

$$a = \left[\frac{Wr}{2}\left(\frac{1}{E_1} + \frac{1}{E_2}\right)\right]^{1/3} \tag{2.1}$$

where r is the radius of the tip and E_1 and E_2 are the Young moduli for the respective surface.
Since $A_C = \pi a^2$ and the pressure $P_C = W/A_C$ we get that $A_C \propto W^{2/3}$ whilst $P_C \propto W^{1/3}$ which is illustrated in Fig. 2.5

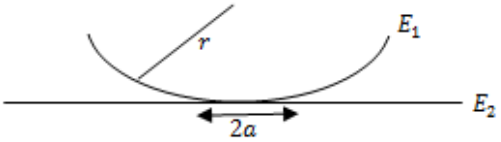

Figure 2.4 Approximation of an asperty tip.

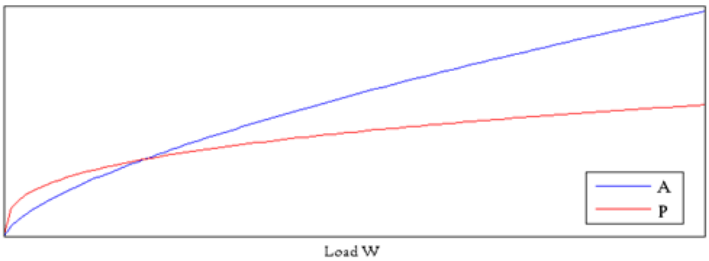

Figure 2.5 Graph showing the elastic deformation, that is the pressure P and area A as a function of an applied load for a sphere pressing on a flat surface.

This results in the fact that as long as the asperity is still in the elastic region, the area of the contact region and thus the total contact area will grow faster than the actual pressure on the material. This is, of course, a very simplified model as several crude approximations are being made. However, with a more detailed model, Boden and Tabor showed a proportionality relation between area and load of $W^{8/9}$. Further, Archard showed that if these asperities in turn are covered by even smaller asperities the proportionality relation is $W^{26/27}$ [Bowden and Tabor, 1964]. The conclusion is that even with elasticity, the area of contact can be almost linearly proportional to the load and thus the normal force on the body. Further, during the relative motion, mechanical energy is converted by friction. The energy dissipates and is mostly transformed into heat, thus creating thermal load. Even though, on a macroscopic scale, the temperature often won't change notably, or at least slowly, on a micro-scale tribological contact the temperature may momentarily change quickly and reach very high values which will affect the strain situation and may even cause instability.

These tribological loads give rise to tribological processes - that is processes that subsume the mechanisms of friction, wear and boundary-layer processes originating from friction and wear.

2.5 Input Variables

The input variables consist of a number of quantities that act on the system or are attributes to the system as a whole when it is executed. They play a key role in the influence of the output variables and are modifiable options in case the output variables need to be optimized. These variables originate from a set of base classes [Grote and Antonsson, 2009]: Type of motion, time sequence of motions, load, velocities, temperatures and loading times. The type of motion mainly consists of sliding, rolling, spin, impact or flowing motion. Time sequences of motions are regular, irregular, back and forth or intermittently. The normal force defines the load. Velocities consist of the relative velocity between the bodies and the ratio of the relative velocity to the average circumferential velocity. Temperatures consist of the body temperature and the effective contact temperature produced during motion. There are also disturbance variables which in some cases need to be taken in account such as vibrations or dust particles, see Fig. 2.1.

2.6 Adhesive contacts

Adhesive forces are weak interactive forces between two bodies that are stronger the closer the bodies are to each other. These forces are important factors in applications where at least one of the contact bodies is made of a soft material, which is valid for polymer laminate. If two neutral atoms (or bodies) positioned at a distance at least the size of the atoms, they will be attracted according to dispersive or van der Waals forces. Two bodies will thus be attracted to each other on the area where their respective atoms are so close to each other that the adhesive forces are strong enough. To move two bodies from a large distance into contact the interaction forces perform a certain work per unit area. This same amount of work must be performed by external forces if the bodies are to be pulled apart. Half of this work is called the surface energy density and is a quantity that determines all of the contact properties related to adhesion. If surfaces would be perfectly smooth, adhesive forces would be big in the macroscopic world. However, surfaces are never perfectly smooth but rather rough even if on different scales. With increased roughness the adhesive forces are decreased significantly, since the number of points in contact will be decreased. Also, the surface energy and the roughness are dependent of the elastic shear modulus. Materials with very small elastic moduli, such as rubber or polymers, will then be able to adhere very rough surfaces.

2.7 The Stribeck Curve

The German professor in mechanical engineering, Richard Stribeck, published a paper in 1902 where he presented his empirical findings of the velocity-pressure-dependence of friction between two liquid lubricated surfaces [Jacobson, 2003].

The results, conducted for different materials on journal bearings, clearly showed a minimum point for the coefficient of friction. This curve was to be called the Stribeck curve, See Fig. 2.7 for experimentally obtained Stribeck curves. Later, from the Stribeck curve, friction for sliding lubricated surfaces has been categorized into three friction regimes, see Fig. 2.6:

1. Solid/boundary friction
2. Mixed friction
3. Hydrodynamic friction

Boundary Friction Low velocity and low viscocity in combination with high load will produce boundary friction. This means that the lubrication consists of little fluid between the solids and a large amount of surface contact.

Mixed Friction Increasing the velocity, the surfaces separate and a fluid film forms in the interface. The thin film supports more and more of the load. The result of the increasing fluid lubrication is a drop in the friction coefficient. This is called the Mixed Friction regime. As the velocity increases the surfaces will continue to separate until there is no more surface contact at which point a friction coefficient minima occurs and there will be a transition into the hydrodynamic friction regime. Now the load is supported entirely by the fluid film.

Hydrodynamic friction Higher velocity will increase the thickness of the film which does increase the reactive force - the fluid drag.

At higher velocities the friction force will remain constant [Popov, 2010].

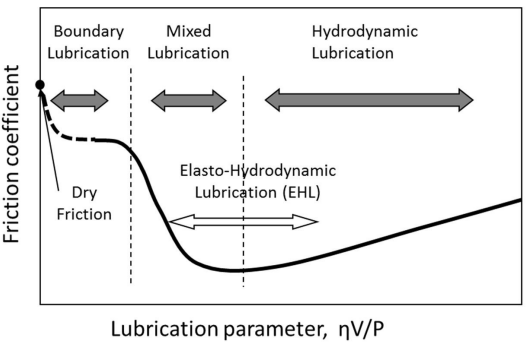

Figure 2.6 Stribeck curve regimes. The horisontal axis shows the usual notation, where η is the velocity, V is the viscosity and P is the pressure. [Kondo et al., 2013]

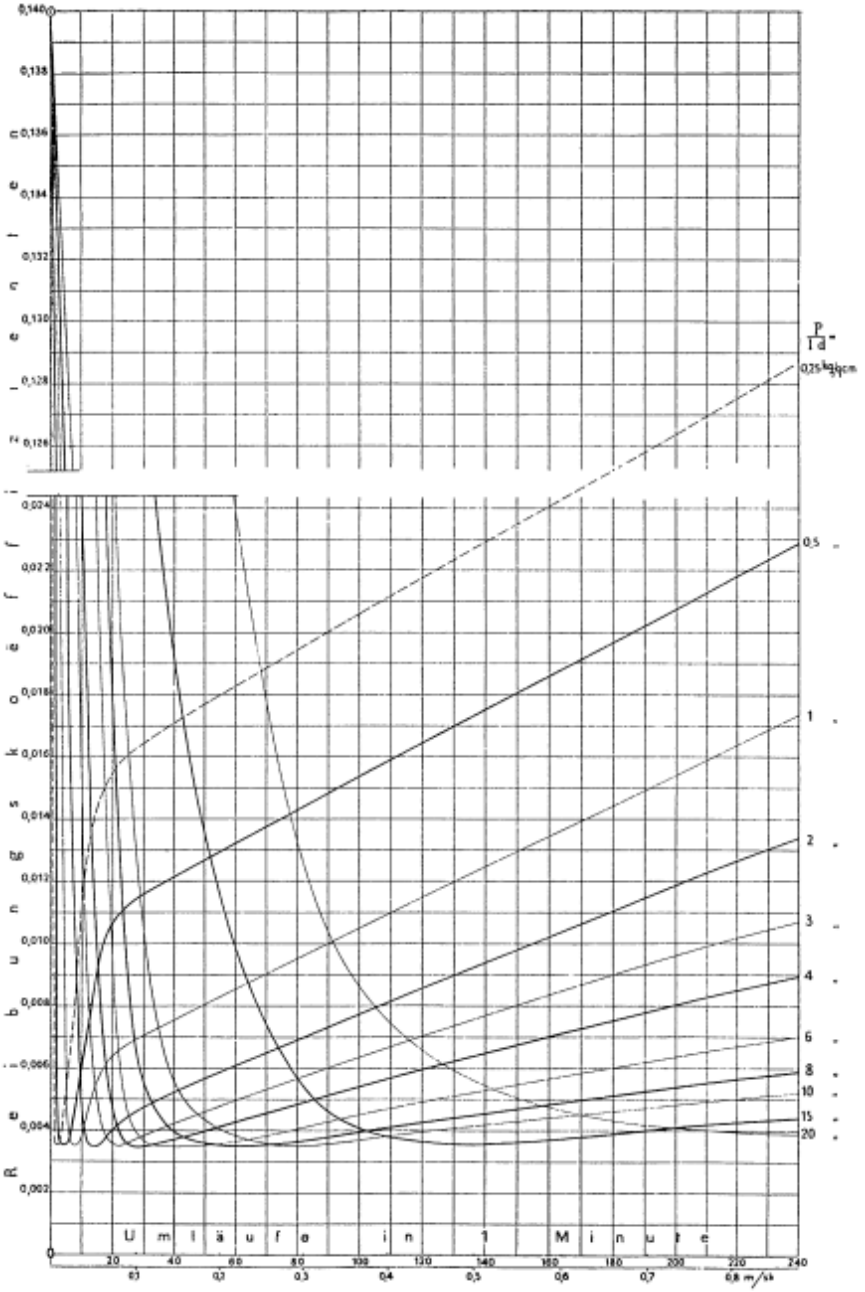

Figure 2.7 Stribeck experimental curves. Journal bearing friction as a function of rotational velocity for different mean pressures [Jacobson, 2003]

2.8 The Bristle Model

The Bristle model is a well established model to describe the contact mechanisms of two surfaces. Two surfaces will make contact at a number of asperities. These are theoretically modelled as two rigid bodies where elastic bristles make out their contact, see Fig. 2.8. When the bodies are moving relative to eachother the bristles in contact deflect, which gives rise to a frictional force - the principle being the same as for springs. At a sufficient force the deflection will be so high that the bristles slip and when enough bristles slip the bodies will enter a sliding regime.

Figure 2.8 The contact mechanics between two bodies is theoretisized as contact between elastic bristles. For simplicity the bristles of the lower body are thought of as rigid and the total elastical properties are therefore accounted for in the top body

2.9 Contact between the nip roller and the material

The material passes through different stations in the laminator on its way from printed carton to laminated material. The key area of interest is the part where the material is driven by a rotating chill roller with applied pressure from a nip roller on the other side, see Fig. 2.9 for a schematic image of the scenario.

The main focus of the friction model is on the nip roller side of the material, that is the contact between the nip roller and the material. The nip roller consists of one thicker rubber material surrounded by a thinner one. The material is clay coated carton. Due to the underlying rubber being compressed by the load of the nip roller against the material (chill roller made of steel) the contact scenario will be simplified to a flat surface in this scenario and for simplicity the tangential forces at the edges will not be accounted for, see Fig. 2.10.

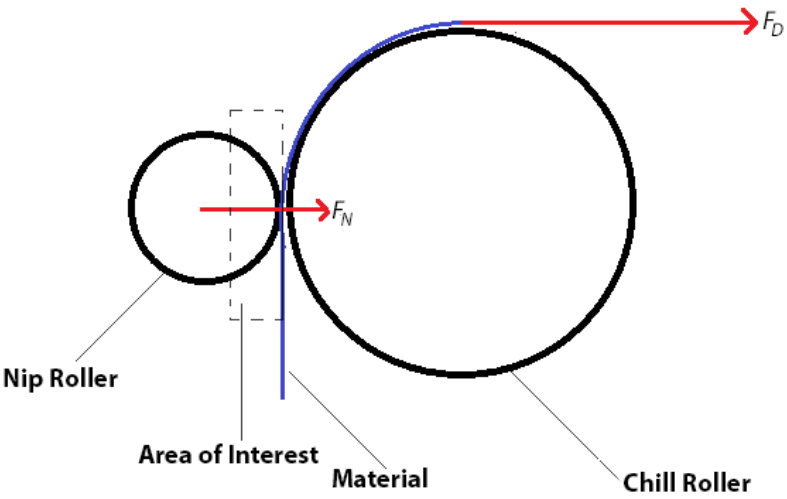

Figure 2.9 Schematic image of the chill roller station.

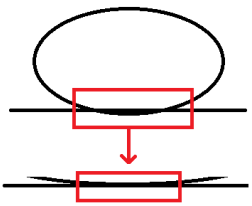

Figure 2.10 The loading case is simplified to two flat surfaces in contact with eachother.

It is estimated that the rotational velocity of the nip roller is about 1% - 2% slower than the one of the chill roller (a maximum of 650 mm/min). Hence the material will 'slip' against the nip roller causing a difference in velocity between the roller and the material - giving rise to friction. It is therefore important to be able to obtain a mathematical model for the friction force that will oppose motion, mainly for simulating purposes but also for control purposes.

2.10 Summary of assumptions and simplifications used for the model

The assumptions used for the system and thus the model due to the explained theory and background can be summarized in the following bullet list:

- A constant sliding velocity of around 1% - 2% of the driving velocity is assumed.
- The pressure situation is considered flat sliding. Any angular effects due to the macroscopic cylindrical shape of the rollers is disregarded for this model.
- The film or coating of the material is a lubricant and dealt with as such. A viscous part must be included in the model.
- The loading case is resembled in a bristle model giving rise to damping and stiffness in the dynamic loading.
- A uniform pressure situation is assumed.
- The friction force is proportional to the applied pressure. This has also been shown to be adequately accurate in a previous (internal) study made. [Oros, 2013]
- As the system runs in one direction with the model will only assume a positive direction ($v > 0$).
- The velocity is assumed to be constant.

3

A Mathematical Formulation

3.1 The LuGre Model

The LuGre model [Wit et al., 1995] is governed by two main equations:

$$\dot{z} = v - \frac{|v|}{g(v)} z \tag{3.1}$$

$$\mu = \sigma_0 z + \sigma_1 \dot{z} + \sigma_2 v \tag{3.2}$$

in which v is the relative velocity between the surfaces, z is the deflection according to the *Bristle Model* (see Fig. 2.8), σ_0 is the stiffness for the deflection/force relationship, σ_1 is the damping coefficient and σ_2 accounts for viscous friction.

In Eq. (3.1) $g(v)$ accounts for the *Stribeck effect* and is given by:

$$g(v) = \frac{1}{\sigma_0}(\mu_c + (\mu_s - \mu_c)e^{-\frac{v^2}{v_s^2}}) \tag{3.3}$$

where μ_c is the kinetic friction coefficient, μ_s is the static friction coefficient and v_s is the Stribeck velocity. Note that here the coefficient of friction are used instead of the force for simplicity. They are obtained by dividing the friction force with the normal force.

Obviously, from Eqs. (3.1) — (3.3) the friction depends on the relative velocity v and is characterized by the six parameters $\sigma_0, \sigma_1, \sigma_2, \mu_c, \mu_s$ and v_s.

3.2 Steady State Model

The *LuGre* model in Sec. 3.1 contains six parameters. Due to the assumptions used for the system (Sec. 2.10) it is natural to reduce the model into steady state, that is $v =$ constant and $\dot{z} = 0$, Eq. (3.1) is set to zero and z can be expressed as:

$$z_{ss} = g(v)sgn(v) \tag{3.4}$$

Inserting Eq. (3.3) into Eq. (3.4) and then into Eq. (3.2) results into an expression for the friction force in steady state:

$$\mu_{ss} = \mu_c sgn(v) + (\mu_s - \mu_c)e^{-\left(\frac{v}{v_s}\right)^2} sgn(v) + \sigma_2 v \tag{3.5}$$

In this case the number of unidentified model parameters is reduced to four (static parameters): μ_s, μ_c, v_s and σ_2. These parameters can be estimated by producing the Stribeck curve from experiments, see Fig. 3.1.

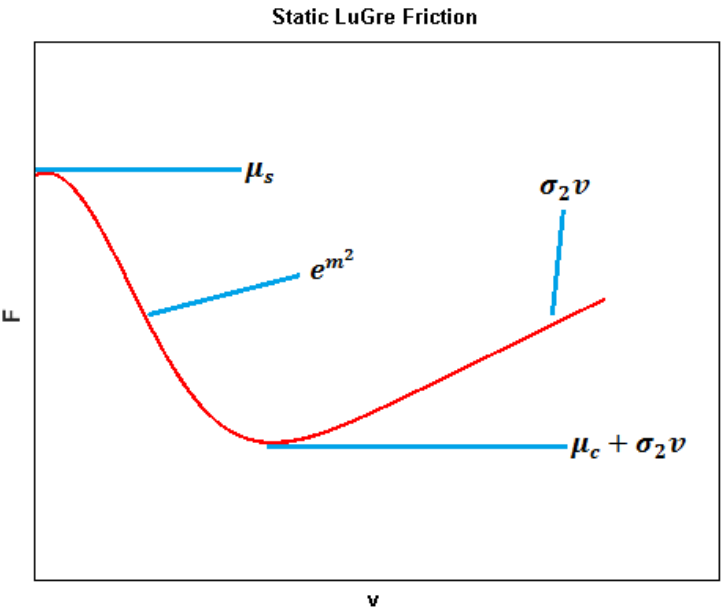

Figure 3.1 Steady State LuGre Friction, where $m = v/v_s$.

The viscous friction function $f_v(v) = \sigma_2 v$ is superposed to the kinetic friction force. This is observed if we let $v \to \infty$. Then Eq. (3.5) becomes

$$\mu_{ss} = \mu_c + (\mu_s - \mu_c)e^{-\infty} + \sigma_2 v = \mu_c + \sigma_2 v \tag{3.6}$$

Figure 3.2 shows how the superposing of the viscous friction creates the linear tail of the curve after the exponential reaches zero and it is evident how the static

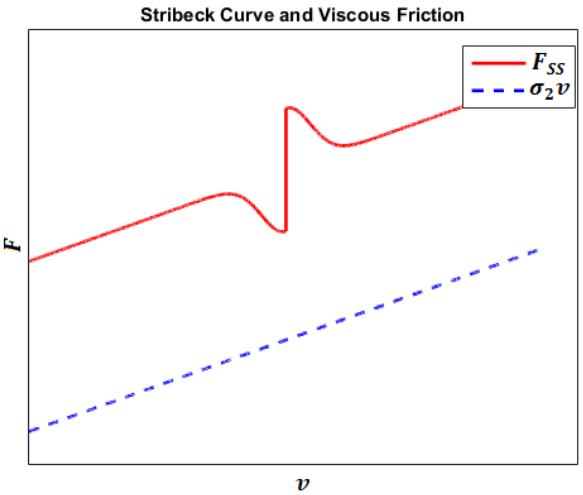

Figure 3.2 Static LuGre Friction and the viscous friction for certain choices of parameters.

LuGre friction model actually models the *Stribeck effect*. The viscous friction will raise the level of the measured kinetic friction by its value.

Figure 3.3 shows a plot of the static friction force for different choices of σ_2.

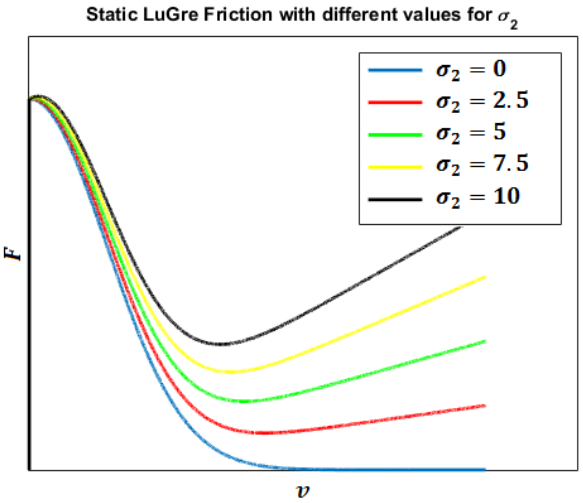

Figure 3.3 Static LuGre Friction with different values of the viscous friction force.

4

Method

4.1 Measurements

The **Instron 5566** is a friction measurement device used for the experiments. See the setup in Figs. 4.1 - 4.2.

Material A is taped on the table, while *Material B* is taped on a sled. The sled is being pulled by a nylon wire through a frictionless pulley with a load cell. A weight may be added onto the sled as an addition to the normal force acting on the materials.
The velocity is constant for the test and the test is repeated three times in order to obtain enough statistical accuracy. The three tests will produce separate raw data outputs (time and force) and also the mean values and standard deviations of the static friction coefficient and the kinetic friction coefficient. *Material A* is the nip rubber sample in the experiments and *Material B* is the carton samples. This will resemble a realistic scenario where the carton and rubber material are in a slip case.

The experiment is repeated for the same type of materials but for different values of velocity, ranging from 0 mm/min to 500 mm/min. Instron 5566 can only measure at one constant velocity at a time. Therefore, instead of continually increasing the velocity, which would be optimal, the curve is produced by increasing the velocity in small steps. This will give discrete points that will be connected into a curve. The measurement data is then collected with velocity and mean dynamic friction force as parameters.

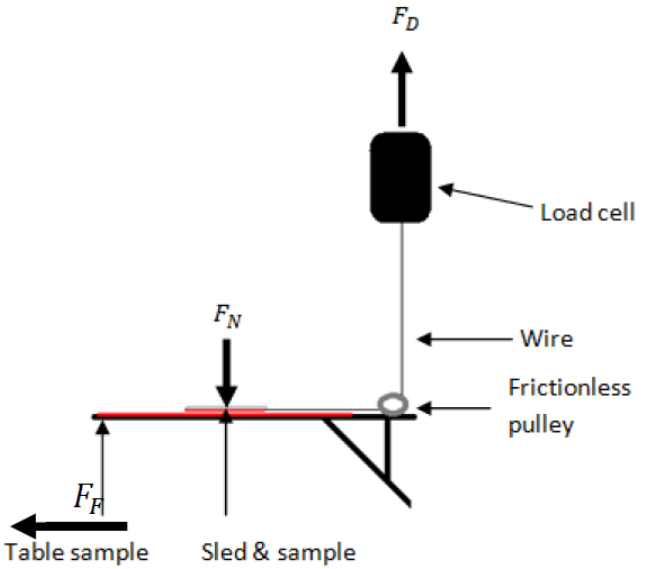

Figure 4.1 Friction measurement setup of Instron 5566. [Oros, 2013]

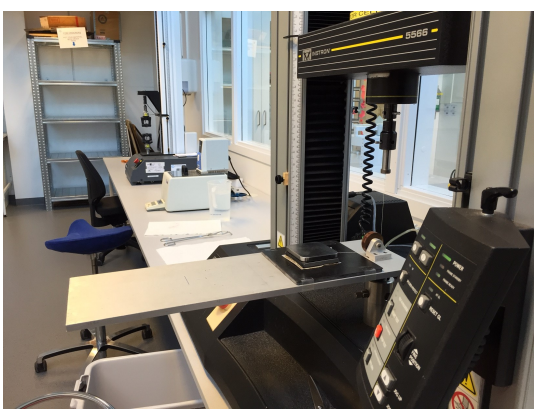

Figure 4.2 Measuring friction between a rubber sample and a carton sample. In the photo it is seen how the load cell pulls the sample along the table surface the table through a frictionless pulley with a nylon wire.

Apart from not being able to produce a continuous increase of the velocity another weakness of this setup is that the sample is not bound to the same position in space for every measure. The only constraint is the nylon wire dragging it into the driving direction. This is further discussed later in Sec. 6.1.

For this project, three experimental studies are conducted:

1. **Initial Minor Study:** Study with few samples.
2. **Pilot Study:** A complete study with pilot samples.
3. **Main Study:** A complete study with a new rubber sample from the supplier and CLC/C carton samples.

The first minor study is done in order to collect samples of data that are used to create routines in MATLAB for data handling and analysis. The pilot study is a complete series of experiments in order to collect enough data to possibly further develop the mathematical model found from the theory to fit the datapoints. The main study is a complete series of experiments using new samples. This is done in order to validate the model created from the pilot study.

4.2 Identification

The parameters in the static LuGre friction model Eq. (3.5) are then identified in the following way—also see Fig. 3.1:

1. Find μ_s by investigating the maximum of the curve.
2. Find $\mu_c + \sigma_2 v$ at the minima of the curve.
3. Find m^2 by fitting the data from the exponential part of the curve $(\mu_{v=0} - \mu_{min})$ by isolating the data and using a curve fitting algorithm.
4. Find $\sigma_2 v$ by fitting the data from the linear part of the curve $(\mu_{min} - \mu_{v_{max}})$ by isolating the data and using a curve fitting algorithm.
5. Find μ_c by withdrawing step 4 from step 2.
6. In step 3 the exponent is denoted δ to give a design freedom.Its value is usually 2, but further in this report it will be denoted δ and given a value depending on the experimental results instead - see Eq. (4.1)

$$\mu_{ss} = \mu_c sgn(v) + (\mu_s - \mu_c) e^{-\left(\frac{v}{v_s}\right)^{\delta}} sgn(v) + \sigma_2 v \tag{4.1}$$

4.3 Data Handling & Modelling

As explained in [Oros, 2013], **Bluehill** (see [*Bluehill Calculation Reference Manual* 2004]) that is the standard software for the Instron 5566 and generates the results from the measurements has some weaknesses.
First of all, the output is given for each measurement as a .pdf file which is not optimal when performing a large number of experiments as in this case. Secondly, it was shown that for smooth transitions between pre-sliding and sliding it generates the wrong breakway friction force resulting in wrong results. In order to resolve these issues a completely new program is written in MATLAB that both collects all data from the experiments and calculates the true mean values of the sliding (dynamic) friction. This is done by applying an alorithm as seen in the scheme in Fig. 4.3 inside the program.

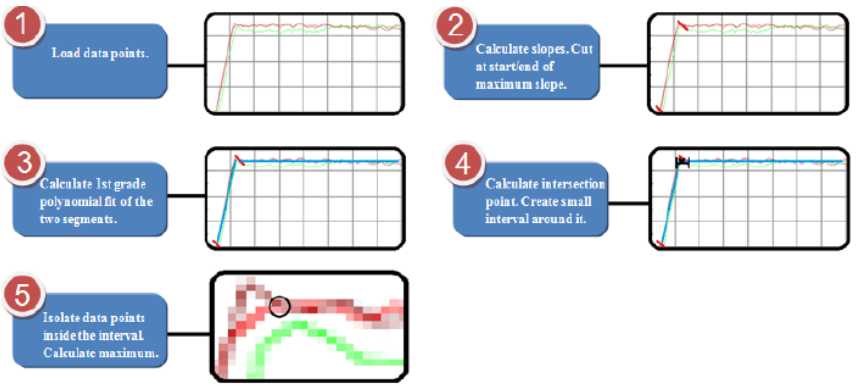

Figure 4.3 Scheme for calculating an exact breakaway friction force and dynamic friction force from the measurements.

The program generates a file containing all relevant data from the experiments. Thereafter MATLAB-scripts are produced in order to find the parameters as described in Sec. 4.2, plot the datapoints and calculate the model values and errors. The error is produced in order to visualize how close the model is to the actual experimental data and is computed as a difference as:

$$e_v = |f_v - g_v| \tag{4.2}$$

f_v being the experimental value of the sliding friction at the velocity v and g_v being the calculated value of the sliding friction at velocity v. The mean error is then calculated in a root mean square sense as:

$$e_{RMS} = \sqrt{\frac{1}{N}\sum_{n=1}^{N}|e_n|^2} \tag{4.3}$$

in which N is the number of data points.

5

Results

5.1 Pilot Study

The first measurements were conducted with a rubber sample from a nip roller and a laminated material from the production, as described in Sec. 4.1. Each sample was measured three times and each velocity was measured three times. Thus for each velocity nine measurements were conducted. The velocity was increased in increments of 10 mm/min ranging from 10 to 500 mm/min. In total this resulted in 150 measurements, see Fig. 5.1 for the collected data of the sliding friction.

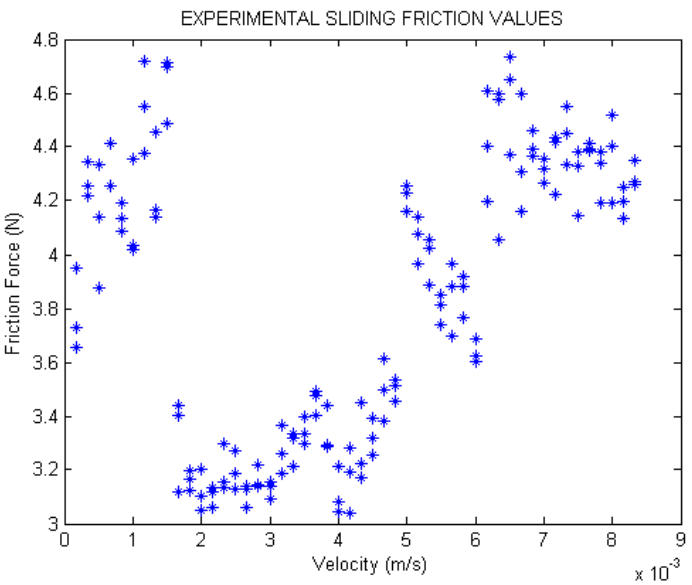

Figure 5.1 Friction force vs sliding velocity

Taking the mean value for each velocity results in Fig. 5.2

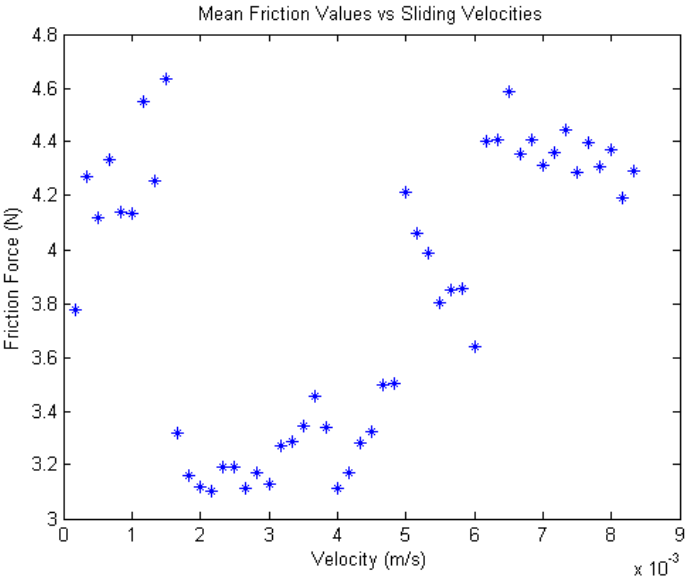

Figure 5.2 Mean friction force vs sliding velocity

The static parameters were identified from the data according to the method described in Sec. 4.2, as shown in Table 5.1 below.

Table 5.1: Parameter values identified from the measured data

Parameter	Notation (Unit)	Value
Static Friction Force	$F_s(N)$	4.4861
Dynamic Friction Force	$F_c(N)$	2.5498
Stribeck Velocity	$v_s(m/s)$	0.0012
Viscous Friction	$\sigma_2(Ns/m)$	230
Design Parameter	$\delta(-)$	2

Using these values in the steady state model Eq. (3.5) results in the following curve, plotted with the mean experimental values in Fig. 5.3 **a)**.

The error was also computed, and plotted as a percentage value of the mean experimental value for each velocity, see Fig. 5.3 **b) c)**.

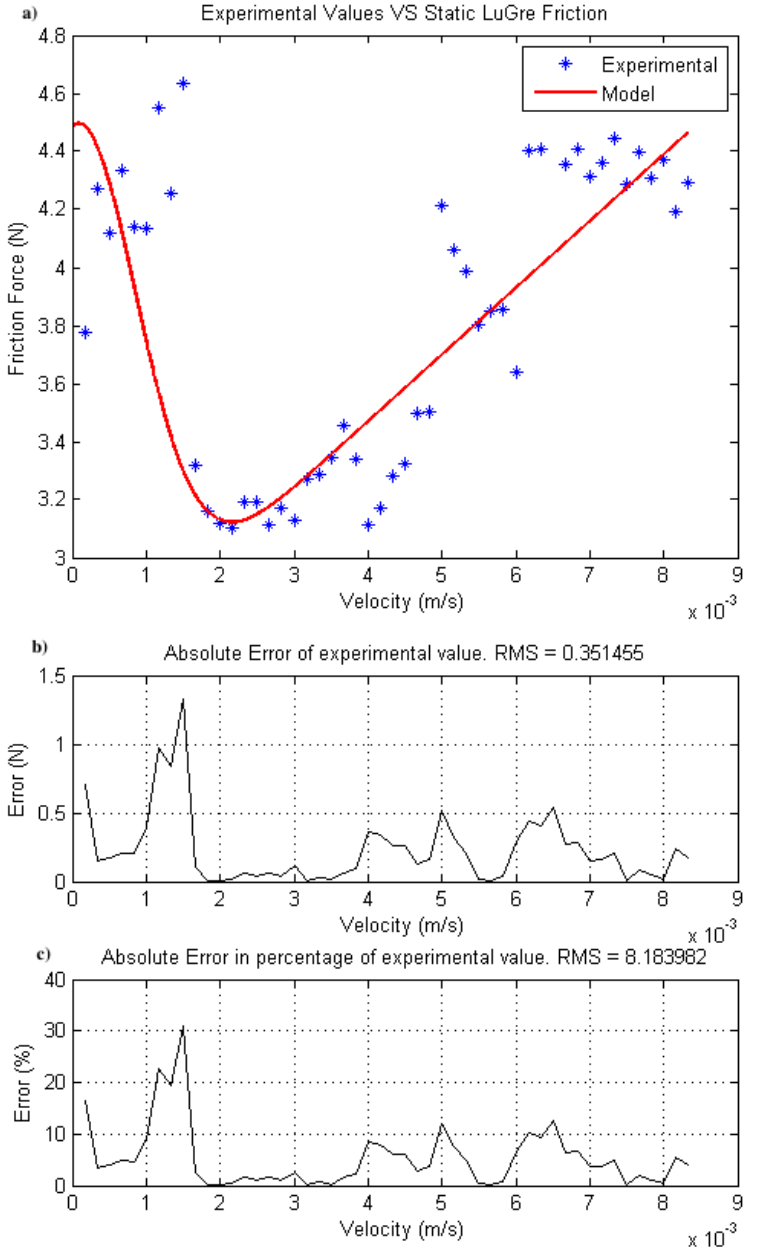

Figure 5.3 **a)** Modelled steady state friction and mean experimental values plotted against velocity. **b)** The absolute error (Experimental value - Model Value). **c)** The absolute error in percentage of the experimental value.

5.2 Main study

For the main study a new rubber sample (Polymate 88A) and CLC/C Carton (Korsnäs Frövi Duplex 260 mN) samples were used. Just as previously in the pilot study each sample was measured three times and each velocity was measured three times. However, the measurements were conducted between 100 mm/min and 500 mm/min. The experimental models are shown in Fig. 5.4

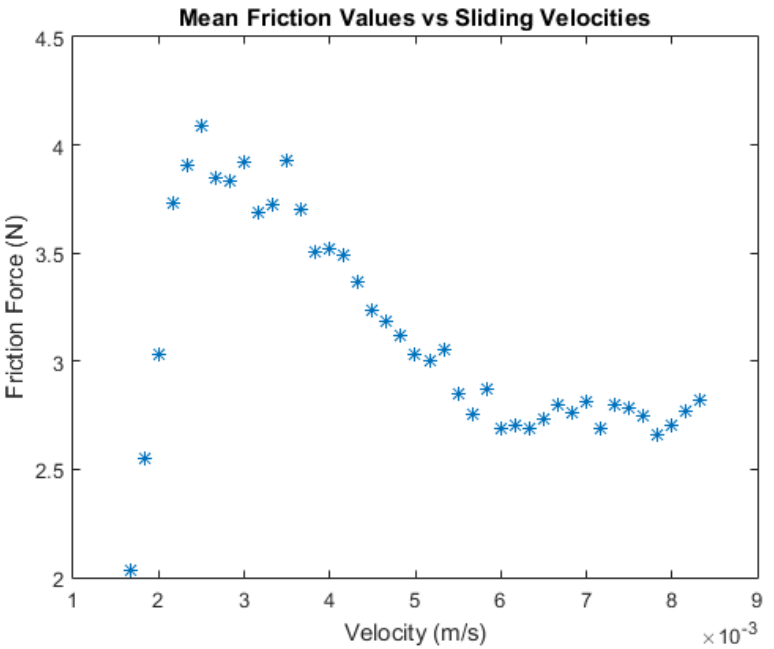

Figure 5.4 Mean friction values vs sliding velocity

From this data the parameter values for the model are identified just as previously, see Table 5.2

Using these parameters, the modelled curve is plotted with the experimental data in Fig. 5.6

Figures 5.6 and 5.7 show how the difference in friction amplitude correlates to the mean sliding friction force in the low velocity region

Table 5.2: Parameter values identified from the measured data.

Parameter	Notation (Unit)	Value
Static Friction Force	$F_s(N)$	4.2672
Dynamic Friction Force	$F_c(N)$	2.6063
Stribeck Velocity	$v_s(m/s)$	0.0049
Viscous Friction	$\sigma_2(Ns/m)$	5
Design parameter	$\delta(-)$	3.2

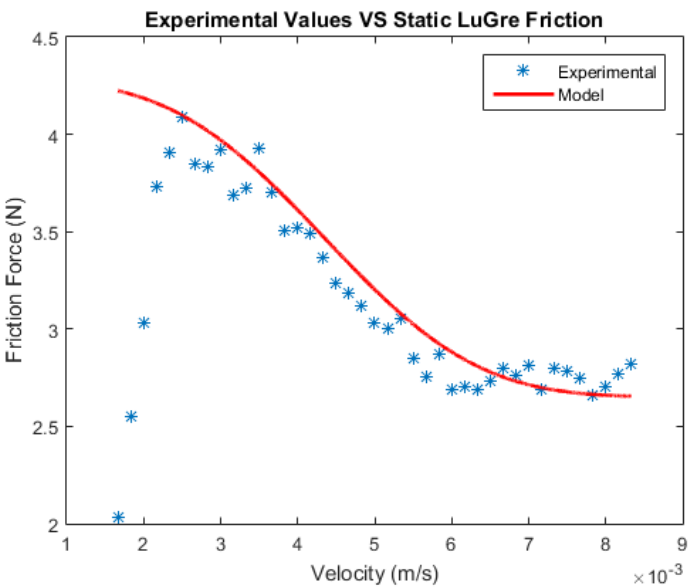

Figure 5.5 Modelled steady state friction and mean experimental values plotted against velocity

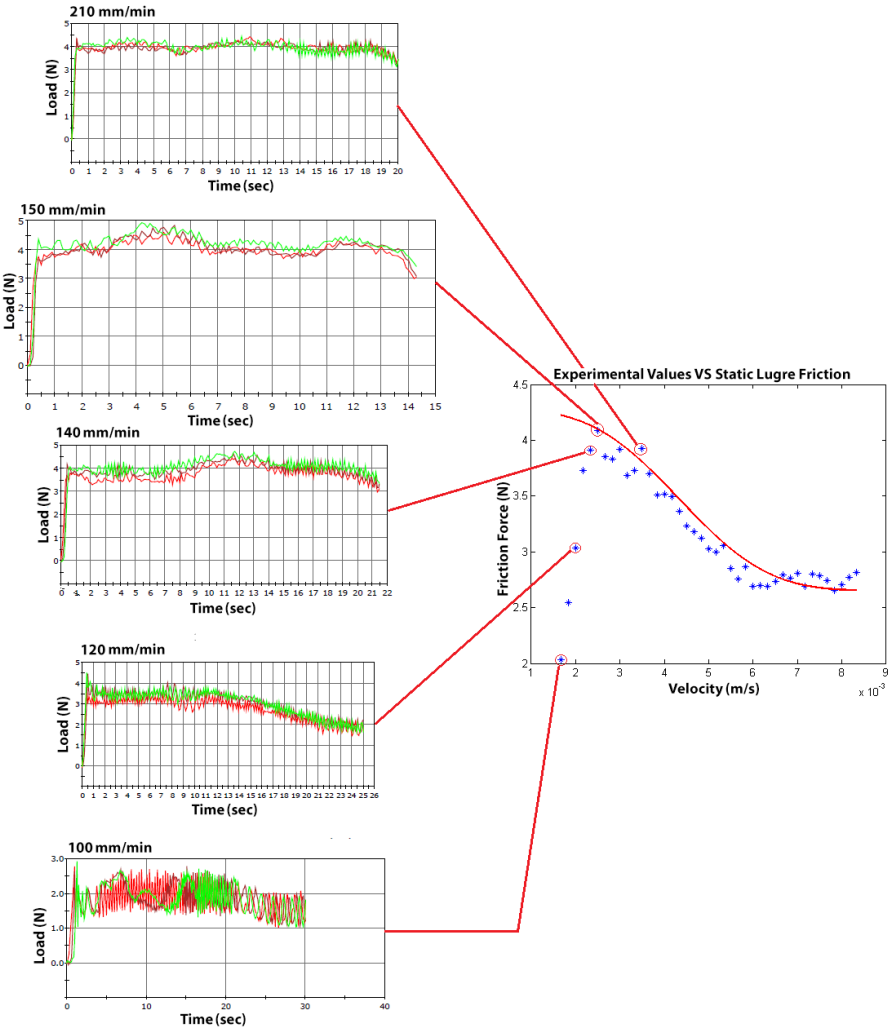

Figure 5.6 Visual presentation of the amplitude difference for the low velocity region and one where the model fits (210 mm/min)

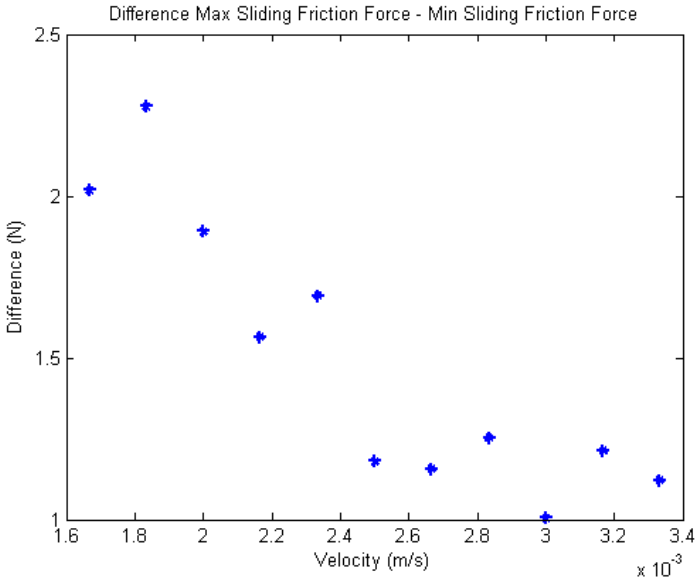

Figure 5.7 Difference between the largest friction value and the lowest, for the velocities between 100 and 200 mm/min.

Fig. 5.8 **a)** shows the model plotted with the experimental data in the ”stable” region ($v > 140 mm/min$).

Fig. 5.8 **b) c)** show the error plots of the stable region.

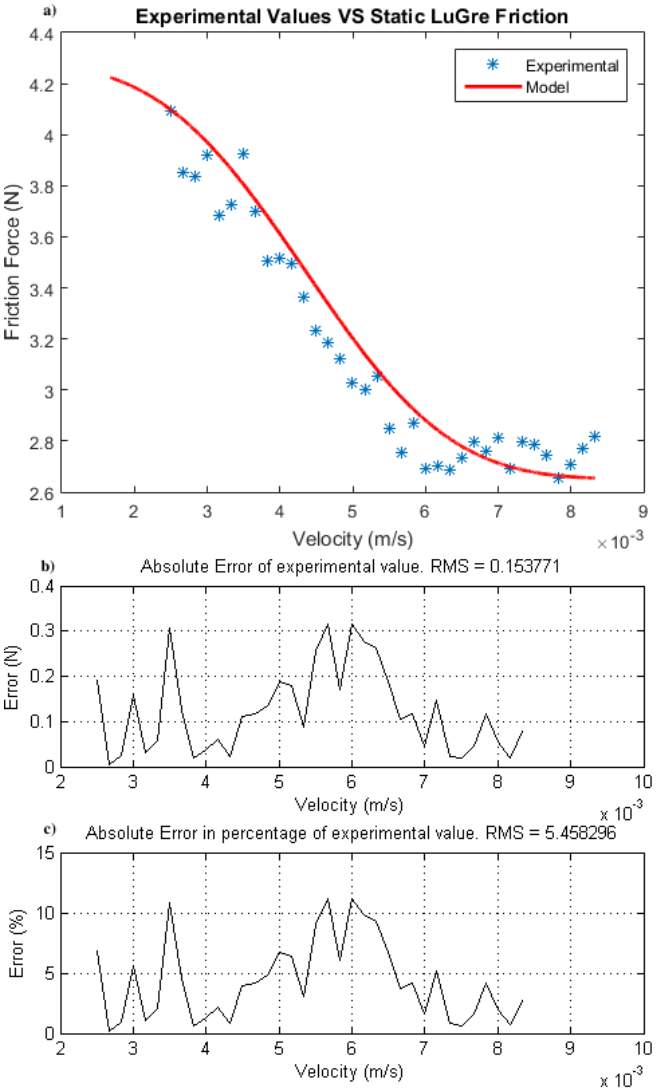

Figure 5.8 **a)** Modelled steady state friction and mean experimental values plotted against velocity. **b)** The absolute error (Experimental value - Model Value). **c)** The absolute error in percentage of the experimental value.

6

Discussion

6.1 Measurements

As explained in Sec. 4.1 the measurement system **Instron 5566** was not entirely ideal for this project. First of all it would be more suitable with a measurement system that is capable of changing the velocity during testing. The main problem with discrete measurement points arises when identifying parameters through curve fitting. For the exponential part of the curve the fitting is performed through a polynomial approximation of the logarithmized data points. Due to this, having discrete points produces a source of error larger than it would naturally be with continuous points. A solution would of course be to use smaller increments for the velocity. However, this is not possible with this device due to the immense time it would take to perform the experiments. Another problem is the degrees of freedom the sample can move. As described in the theory the frictional value is very dependent on the actual coordinate in space due to the highly irregular surface characteristics that affect it. With this setup the only constraint is the general direction of the velocity which we will call the y-direction (obviously it is also constrained vertically in the z-direction). However, it will move freely in the x-direction, as seen in Fig. 6.1.

Figure 6.2 shows the rubber sample used in the main study. As seen the surface is not geometrically homogenous on a macroscopic scale either. These irregularities will push the carton sample in different directions depending on where the sample is initially placed and thus its path. Even though the operator could be very careful with placing the sample in the very same spot every time, there is still a source of uncertainy. This issue could perhaps be overcome by adding more pressure on the sample but the measurement setup does not support that.

6.2 Pilot & main studies

As seen in Fig. 5.3 the modeled curve seems to follow the measured data well. The viscous friction is very dependent on position which explains the dispersion. This is also shown in Fig. 5.3 which shows the error both as a ratio and as a percentage

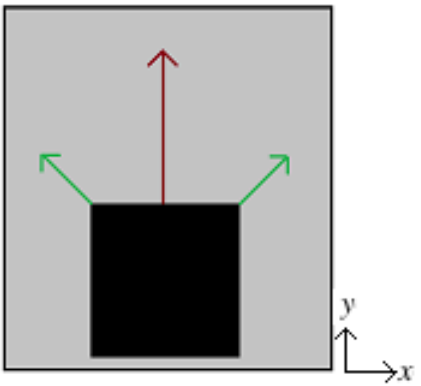

Figure 6.1 The sample (black) is constrained in the y-direction due to the nylon wire (as indicated by the middle red arrow) but will be able to move freely in the x-direction (outer green arrows) due to surface irregularities.

Figure 6.2 The rubber sample used in the main study.

measure of the experimental values at the different velocities. The RMS error is 8%, much due to the initial peaks. These peaks are further discussed in Sec. 6.3. The pilot study showed that the model fits for the experimental setup and thus also work for the nip roller model.

As seen in the results from the pilot study and more evident in the results from the main study (Fig. 5.6) the model follows the experimental data well except in the very low velocity region which is called the unstable region ($v \leq 140$ mm/min). In the pilot study an initial assumption was that this was due to uncareful measurements at low velocities. However the main study showed it is due to the heavy friction induced oscillations occuring for those velocities—see how there is an almost linear relationship between the decreasing estimated amplitude and the increasing velocity up to the stable region in Fig. 5.7. It seems that due to this fact the mea-

suring system might not be adequate for this kind of friction induced oscillations. Given the initial assumptions for the system and the model as described in Sec. 2.10 this unstable velocity-region is lower than what is required of the model. It is also seen how the friction values plateau at a certain velocity in both measurements (Figs. 5.2 and 5.4), $v = 0.0065$ and 0.006 m/s respectively. This indicates that after these values the friction force will maintain a stable value for the upcoming velocities (until reaching really high velocities), as theory describes.

6.3 Low velocity errors

As it appeared in the results for the very low velocities the model values diverged a lot from the experimental values, which is also shown in Fig. 6.3.

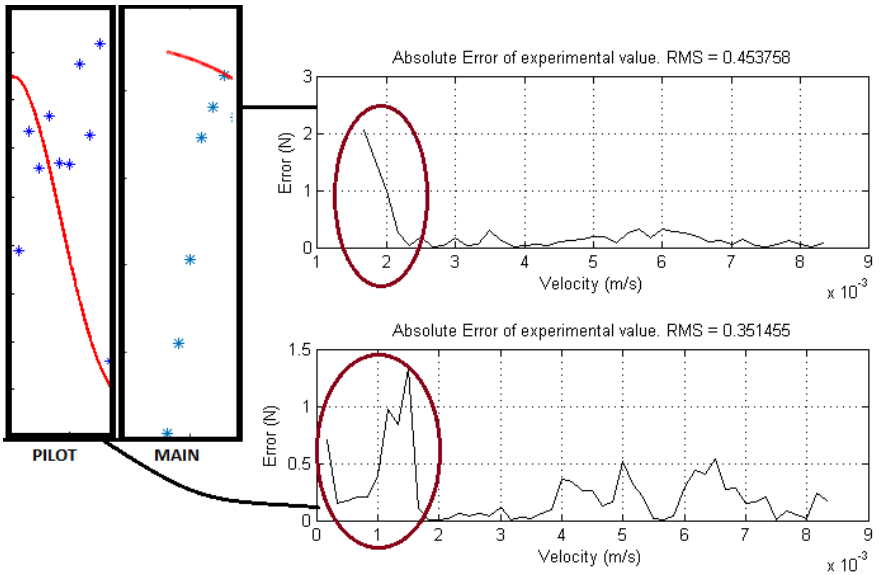

Figure 6.3 Low velocity errors for the pilot and main study.

Even though it is already said that this domain of velocity is not of interest to the application itself, it is interesting to take a look at the effects in this discussion. Another experiment was done measuring for these low velocities in both directions according to [Johansson et al., 2000], see Fig. 6.4.

In Fig. 6.5 it is evident how the friction force is concentrated around one range of values but the spread is larger the closer to zero velocity the experiment is done.

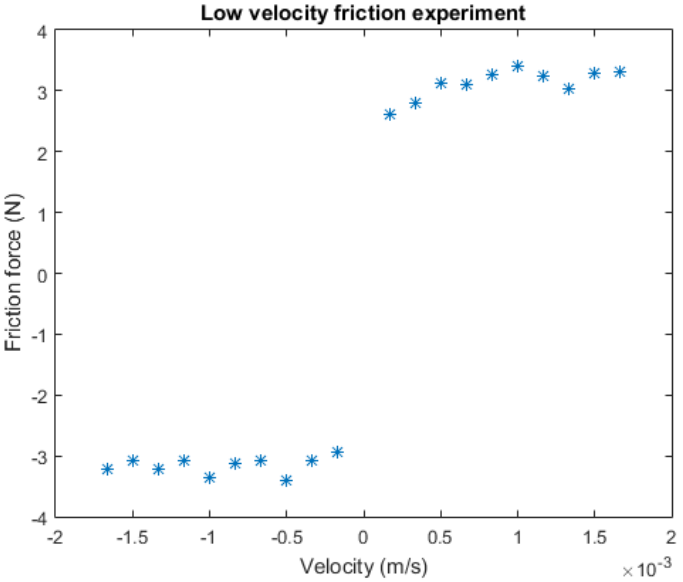

Figure 6.4 Low velocity experiment.

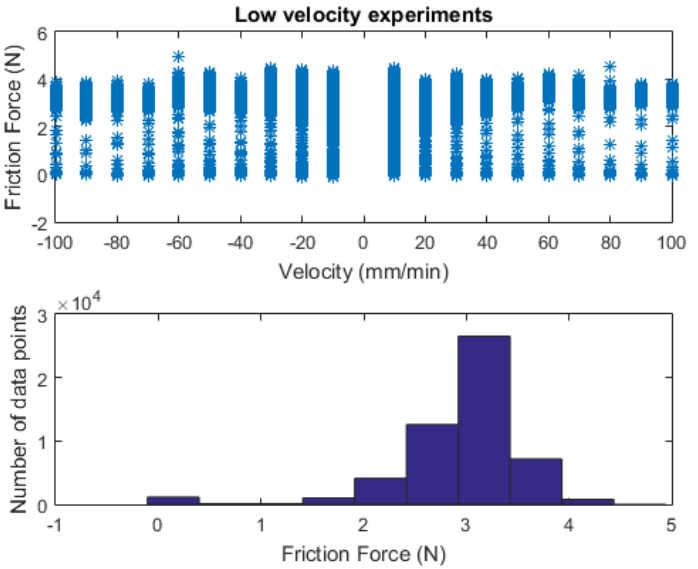

Figure 6.5 Distribution of the friction force for the low velocity experiments.

The same rubber sample and type of CLC/C carton samples as in the main study were used and it can be seen that the friction force follows the same pattern as in the main study. It was seen that there seems to be large friction induced oscillations in this velocity range, see Figs. 5.6 and 5.7. What happens during the sliding is that the sample will be pulled back by enough friction force to make it stop motion until a greater force is pulling it so it overcomes the friction and starts sliding again. This is repeated during the motion and the effect is called stick-slip [Olsson, 1996]. It is seen as if the sample "jumps" across the rubber sample instead of just sliding. This effect appears on any surface sliding on another surface. However for smooth sliding it appears as micro-stick-slip,that is, very small oscillations. In our case, it was macro-stick-slip greatly affecting the measurement data. This sliding is dominated by dynamic features such as damping and stiffness and that is why the model does not capture the effect, as it is static. If one would like to capture this effect as well, the dynamic model would have to be used. In order to do this a measurement setup that can increase the velocity would have to be used together with a method such as the one described in [Johansson et al., 2000].

As a conclusion, when having done the necessary measurements for the chosen set of materials and the model has been established, a range of velocities where it is valid should be given. In such case, one should know that the model does not apply for the lower velocities when intense oscillations are experienced, and that after the higher limit the friction value will be maintained.

6.4 Applicability in simulations

The steady state-model will always return one value that will be the estimation of a force countering motion. Therefore, it will be very easy to add in simulations as there will be no numerical issues around it. The engineer performing the simulation will have to keep in mind, though, the simplifications mentioned in Sec. 2.10 that lead to the model. Also, the velocity domain for which the model applies must be respected in order to achieve good results. Another thing to keep in mind is that friction is usually not given as a fix value, but in ranges. This is due to the impact of the surroundings (e.g., temperature) and surface characteristics (see Sec. 6.1) but also due to oscillations that occur. When calculating the dynamic friction value from the experimental data it is the mean value of the measurement data, see Fig. 6.6.

As seen on most measured points in time the friction value deviates a bit from the actually produced value.

6.5 Other work

Friction has been studied a lot in the vehicle and tyre industry for obvious reasons. However there is not a lot of other work done on modelling friction when it comes to the specific types of materials that are dealt with in this thesis. Much of the work

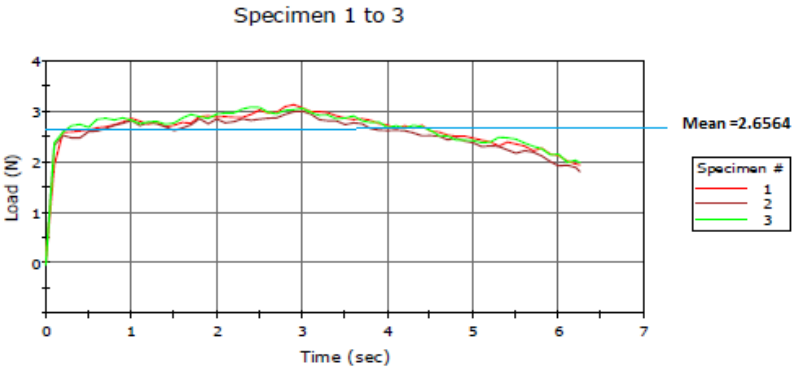

Figure 6.6 The red, dark red and green curves are the measurement data during sliding. The blue line is the mean value produced.

revolves around the LuGre model and further development of the dynamics in it and a lot of the work is done for control purposes. See for instance [Alvarez-Icaza and Jiménez-Fabián, 2007] and [Swevers et al., 2000].

7

Conclusions

7.1 Objectives & Future Work

As described in Sec. 1.2 the main goal was to find a mathematical model describing the friction behaviour in the nip. With the aid of background and theory, two requirements were set up in order to fulfill this goal. The steady-state model Eq. (3.5) takes the velocity as its input parameter and gives a kinetic friction coefficient as output - thus the first requirement is met. In order to make this possible, three other input parameters must be identified. A method for this was described in Sec. 4.2. Therefore the requirements for the thesis have been fulfilled. However, this model can be developed further in future studies. By using a measurement setup that can continuously increase the velocity, giving a continuous velocity graph instead of one with discrete points, would immensely improve the accuracy of the model as the polynomial fitting algorithms that are more accurate the more data points that are used. Further investigating the dynamic part of the model and how to identify the damping and stiffness parameters would allow for the model to describe pre-sliding sufficiently and thus also describing the low-velocity oscillations. Also, this would make it possible to describe changes in the velocity. The cylindrical case gives rise to other effects in the contact case and thus also friction case. In order to completely describe the situation in the nip, the angular case in the boundary of the contact situation must also be evaluated and described. This being said, the simplifications made for this project do not make the model insufficient as the constant velocity assumption and the flat surface assumption accounts for the biggest part of the friction case in the nip.

Bibliography

.

Alvarez-Icaza, L. and R. Jiménez-Fabián (2007). *An identifiable control-oriented dynamic friction model*. Nonlinear Control Systems, Vol. 7, pp.164—169.

Barthel, E. (2008). *Adhesive elastic contacts - JKR and more*. Journal of Physics D: Applied Physics, vol. 41, p.163001. URL: http://stacks.iop.org/0022-3727/41/i=16/a=163001.

Bluehill Calculation Reference Manual (2004). Instron.

Bowden, F. and D. Tabor (1950). *The friction and lubrication of solids Part I*. Oxford University Press, London.

Bowden, F. and D. Tabor (1964). *The friction and lubrication of solids Part II*. Oxford University Press, London.

Grote, K. and E. Antonsson (2009). *Springer Handbook of Mechanical Engineering*. Springer-Verlag, Berlin Heidelberg.

Jacobson, B. (2003). *The Stribeck Memorial Lecture*. Tribology International 36, pp. 781-789.

Johansson, R., A. Robertsson, K. Nilsson, and M. Verhaegen (2000). *State-space system identification of robot manipulator dynamics*. Mechatronics 10, pp.403—418.

Kondo, Y., T. Koyama, and S. S. (2013). *Tribological Properties of Ionic Liquids — New Asepcts for the Future*. InTech. DOI: 10.5772/52595.

Olsson, H. (1996). *Control Systems with Friction*. PhD thesis ISRN LUTFD2/TFRT--1045--SE. Department of Automatic Control, Lund University, Sweden.

Oros, S. (2013). *'Evaluation of Instron 5566 as a testing asset for measuring friction on packaging material*. Tetra Pak (Internal Report) DR28819.

Persson, B. (1998). *Sliding Friction*. Surface Science Reports.

Popov, V. (2010). *Contact Mechanics and Friction - Physical Principles and Applications*. Springer-Verlag: Berlin Heidelberg.

Swevers, J., F. Al-Bender, Ganseman.C.G., and T. Prajogo (2000). *An Integrated Friction Model Structure with Improved Presliding Behavior for Accurate Friction Compensation*. IEEE Transactions on Automatic Control, Vol. 45, No. 4, pp.675—686.

Wit, C. de, H. Olsson, K. Åström, and P. Lischinsky (1995). *A New Model for Control of Systems with Friction*. IEEE Transactions on Automatic Control, vol. 40, no. 3, pp. 419-425.

Lund University
Department of Automatic Control
Box 118
SE-221 00 Lund Sweden

Document name
MASTER´S THESIS

Date of issue
June 2015

Document Number
ISRN LUTFD2/TFRT--5968--SE

Author(s)
Stefan Oros

Supervisor
Rolf Johansson, Dept. of Automatic Control, Lund University, Sweden
Anders Robertsson, Dept. of Automatic Control, Lund University, Sweden (examiner)

Sponsoring organization

Title and subtitle

A Friction Model for Laminator Nips

Abstract

The main objective for the thesis project is to find a suitable mathematical model of the velocity dependent friction force that arises between the nip roller and the carton material in the laminator at slip, in order to enable realistic simulations of the nip in the laminator. Theoretically, the LuGre model is found to contain the necessary physical properties for the actual situation. Experiments are conducted measuring friction between a rubber sample and carton samples in order to find an expansion and validation of the model. The model is found to produce a satisfactory low-magnitude residual in relation to the experiments for the range that varies with velocity. During the low velocities high-amplitude friction induced oscillations appear making the measurements highly inaccurate. It is known, however, that the slip will never reach these low velocities so this source of error is disregarded. Also, the measurement instrument is found not to be entirely ideal for this project. An instrument that can continuously change the velocity would be better. This model is good for most of the nip cases. However, further investigations are needed for the boundary effects that arise due to the cylindrical shape of the rollers and also a way to identify the dynamical parameters and thus expand from a steady-state model to a dynamical model.

Keywords
friction, LuGre, modelling, Stribeck, sliding, carton

Classification system and/or index terms (if any)

Supplementary bibliographical information

ISSN and key title
0280-5316

ISBN

Language
English

Number of pages
1-38

Recipient's notes

Security classification